HHS Public Access

Author manuscript

Cell Metab. Author manuscript; available in PMC 2016 August 04.

Published in final edited form as:

Cell Metab. 2015 August 4; 22(2): 266–278. doi:10.1016/j.cmet.2015.06.007.

Targeted Induction of Ceramide Degradation Leads to Improved Systemic Metabolism and Reduced Hepatic Steatosis

Jonathan Y. Xia[#1], **William L. Holland**[#1], **Christine M. Kusminski**[1], **Kai Sun**[1], **Ankit X. Sharma**[1], **Mackenzie J. Pearson**[1], **Angelika J. Sifuentes**[1], **Jeffrey G. McDonald**[2], **Ruth Gordillo**[1], and **Philipp E. Scherer**[1,3,†]

[1]Touchstone Diabetes Center, Department of Internal Medicine, The University of Texas Southwestern Medical Center, Dallas, Texas 75390-8549

[2]Department of Molecular Genetics, The University of Texas Southwestern Medical Center, Dallas, Texas 75390-8549

[3]Department of Cell Biology, The University of Texas Southwestern Medical Center, Dallas, Texas 75390-8549

[#] These authors contributed equally to this work.

Abstract

Sphingolipids have garnered attention for their role in insulin resistance and lipotoxic cell death. Aberrant accumulation of ceramides correlates with hepatic insulin resistance and steatosis. To further investigate the tissue-specific effects of local changes in ceramidase activity, we have developed transgenic mice inducibly expressing acid ceramidase, to trigger the deacylation of ceramides. This represents the first inducible genetic model that acutely manipulates ceramides in adult mouse tissues. Hepatic overexpression of acid ceramidase prevents hepatic steatosis and prompts improvements in insulin action in liver and adipose tissue. Conversely, overexpression of acid ceramidase within adipose tissue prevents hepatic steatosis and insulin resistance. Induction of ceramidase activity in either tissue promotes a lowering of hepatic ceramides and reduced activation of the ceramide-activated protein kinase C isoform PKC-zeta. These observations suggest the existence of a rapidly acting "crosstalk" between liver and adipose tissue sphingolipids, critically regulating glucose metabolism and hepatic lipid uptake.

[†]Correspondence should be addressed to: Touchstone Diabetes Center, Department of Internal Medicine, University of Texas Southwestern Medical Center, 5323 Harry Hines Blvd., Dallas, TX, 75390-8549, USA, Philipp.Scherer@utsouthwestern.edu, Tel: 214-648-8715. Fax: 214-648-8720.

The authors declare no conflicts of interest.

Author contributions

JYX and WLH are co-first authors. JYX (liver results) and WLH (adipocyte results) designed the studies, carried out the research, interpreted the results, and wrote the manuscript. CMK, KS, AXS, MJP, AJS, JGM and RG assisted in study design, performed research, and reviewed the manuscript. PES designed the study, analysed the data, reviewed and revised the manuscript, and is responsible for the integrity of this work. All authors approved the final version of the manuscript

Introduction

Numerous studies in humans and animals have shown that hepatic steatosis is strongly associated with insulin resistance. Mice challenged with a high-fat diet develop severe insulin resistance and hepatic steatosis (Birkenfeld and Shulman, 2014; Shimomura et al., 1999a; Shimomura et al., 1999b). However, the causal relationship between hepatic steatosis and insulin resistance is unclear and controversial. Murine models with altered hepatic lipid storage (Monetti et al., 2007; Yu et al., 2005), mobilization (Brown et al., 2010; Hoy et al., 2011; Minehira et al., 2008) and oxidation (Monsenego et al., 2012) all exhibit greatly increased hepatic lipid accumulation without accompanying insulin resistance. Conversely, alterations in hepatic insulin signaling are sufficient to induce hepatic steatosis (Taniguchi et al., 2005).

Ceramides are important members of the sphingolipid family and are essential precursors for complex sphingolipids. A series of studies have shown that increased ceramide levels in both liver and plasma coincide with the development of liver dysfunction, hepatic insulin resistance, and steatosis in rodents (Ichi et al., 2007; Xia et al., 2014; Yetukuri et al., 2007). Previous work has identified the liver as a target of ceramide-induced insulin resistance and inhibition of whole-body ceramide synthesis reduces obesity-induced insulin resistance in rodents (Holland et al., 2007). In particular, ceramides derived from C16 fatty acids appear to oppose insulin action most potently (Raichur et al., 2014; Turpin et al., 2014). Breakdown of ceramides are initiated by enzymes called ceramidases, which are categorized by homology and pH optima at which they can hydrolyze ceramides into sphingosines and free fatty acids (Xia et al., 2014). The anti-diabetic and anti-steatotic adipokine, adiponectin rapidly lowers hepatic ceramide content, thereby improving glucose homeostasis through its receptor-associated ceramidase activity (Holland et al., 2011). Similarly, overexpression of acid ceramidase in cultured cells prevents saturated fatty acids from impairing insulin action in cultured C2C12 myotubes (Chavez et al., 2003).

Previous studies on the role of sphingolipid biosynthetic enzymes in systemic metabolism have employed constitutive gain-of-function or loss-of-function models. However, the usefulness of these constitutive models has been limited by complex phenotypes due to compensatory mechanisms and developmental issues. To further investigate the physiological effects of an acute increase in ceramidase activity in a tissue-specific manner, we have developed transgenic mice that express acid ceramidase under the control of a tetracycline response element cell type-specifically. This allows us to induce ceramide deacylation in response to doxycycline exposure, resulting in the degradation of ceramides made within the cell or following uptake from serum. These models reveal profound improvements in hepatic steatosis and glucose metabolism with strong evidence for interorgan cross-talk as sphingolipids are shunted back and forth between liver and adipose. Thus, this system enables us, for the first time, to probe the impact of a genetically-induced, acute change in ceramide levels on local and systemic insulin sensitivity.

Results

Overexpression of acid ceramidase in the liver reduces hepatic ceramide levels and improves hepatic and adipose insulin sensitivity

Myriocin, an inhibitor of *de novo* ceramide synthesis, also robustly protects against hepatic steatosis when wildtype mice are maintained on a high fat diet (Supplemental Fig. 1A). To disrupt the over-accumulation of ceramides in the liver, we generated an inducible, liver-specific acid ceramidase transgenic (Alb-AC) mouse, which combines three transgenic lines: the albumin promoter-driven Cre line, a transgenic line carrying a Rosa26 promoter-driven loxP-stop-loxP-reverse tetracycline-controlled transactivator (rtTA) gene, and a Tet-responsive human acid ceramidase transgenic line (TRE-AC) (Supplemental Fig. 1B). In the absence of doxycycline, there is no AC transgene expression in the liver when using a primer set that recognizes both human and mouse acid ceramidase sequences equally well. Upon treatment with doxycycline, AC gene expression in the triple transgenics reaches approximately four times the levels seen in wild-type (WT) littermates. The overexpression is liver-specific, as it is not detected in any other tissues (Supplemental Fig. 1C). The increase in hepatic AC mRNA levels resulted in a three-fold increase in acid ceramidase enzyme activity in the liver (Supplemental Fig. 1D). Serum ceramidase activity was not changed between WT and Alb-AC mice after doxycycline induction (Supplemental Fig. 1E).

We challenged the WT and Alb-AC mice with a high fat diet (60% calories from fat) containing 200mg/kg doxycycline (HFD-dox). After 8 weeks of HFD-dox exposure, wildtype mice showed a 2.4 fold increase in hepatic ceramides compared to chow-fed controls (Supplemental Fig. 1F). Alb-AC mice showed a significant reduction in $C_{16:0}$ and $C_{18:0}$ *hepatic* ceramide species (Fig. 1A). In parallel, a significant lowering of $C_{16:0}$ and C18:0 ceramide species was also observed in the *serum* (Fig. 1A). Interestingly, although levels of *liver* sphingoid species did not change significantly compared to WT except for the levels of sphingosine, *serum* sphingoid species exhibited a sharp decline compared to WT (Supplemental Fig. 1G). Since past evidence showing the negative correlation between the signaling lipid diacyglycerol (DAG) and hepatic steatosis and insulin resistance (Shulman, 2014), we also measured hepatic levels of DAGs. Surprisingly, we found that levels of DAG in the liver were significantly higher in our Alb-AC mice compared to WT (Fig. 1B). Transcriptionally, we found mRNA levels of DGAT1 decreased to 30% of WT, while levels of DGAT2 increased to almost five-fold above WT levels (Supplemental Fig. 1H). Serum levels of DAGs were comparable between WT and Alb-AC mice (Fig. 1B).

We exposed Alb-AC and WT littermate control mice to HFD-dox for 8 weeks. We observed similar weight gain curves for the Alb-AC and WT mice and comparable body weights at the end of the 8 weeks of HFD-dox exposure (Supplemental Fig. 1I). However, compared to WT controls, Alb-AC mice exhibited significantly reduced blood glucose levels during the oral glucose tolerance test (OGTT) (Fig. 1C), indicating an improvement in systemic glucose tolerance. Additionally, the plasma insulin levels during the OGTT were also markedly lower in the Alb-AC mice (Fig. 1D). Furthermore, HFD-dox-fed Alb-AC mice also had substantially decreased blood glucose levels after insulin injection during an insulin tolerance test (ITT) (Fig. 1E), suggesting enhanced insulin sensitivity.

We performed hyperinsulinemic-euglycemic clamp studies. The glucose infusion rate needed to maintain euglycemic conditions (~150 mg/dl) was increased in Alb-AC mice compared to their littermate controls (Fig. 1F**, left panel**), demonstrating that whole-body insulin sensitivity is improved. Whole body glucose disposal was not altered (Supplemental Fig. 1J), suggesting minimal effects on muscle insulin action. There were no significant changes in lipolysis between WT and Alb-AC mice under clamped or under insulinopenic conditions where insulin-induced suppression of lipolysis is more pronounced (Table 1, Supplemental Fig. 1K). Hepatic glucose production under hyperinsulinemic clamp conditions was suppressed more efficiently in Alb-AC mice (Fig. 1F**, right panel**). Specifically, hyperinsulinemic clamp conditions suppressed hepatic glucose production of Alb-AC mice by ~47% compared to ~15% of WT mice (Supplemental Fig. 1L). Insulin signaling in the liver and adipose tissue was assessed by insulin-stimulated phosphorylation of Akt. p-Akt levels were greatly increased in the liver of transgenic animals. Moreover, even though the increase in ceramidase activity is restricted to hepatocytes, insulin-stimulated p-Akt in gonadal adipose tissue was also elevated (Fig. 1G). Consistent with these observations, 2-deoxyglucose uptake during clamped hyperinsulinemic conditions showed that the gonadal (gWAT), subcutaneous (sWAT) and mesenteric (mWAT) fat pads of Alb-AC mice had increased 2-deoxyglucose uptake compared to WT (Fig. 1H). Differences in glucose disposal and glucose production could not be explained by minimal differences in body weight or concentrations glucose and insulin during the clamped state (Table 1).

Overexpression of AC in the hepatocyte prevents HFD-mediated hepatic lipid accumulation and attenuates adipose tissue inflammation and fibrosis

While the HFD causes a marked increase in the liver weights of both Alb-AC and WT mice, the livers from Alb-AC mice are qualitatively smaller and less lipid-laden compared to WT (Fig. 2A**, left**). The weights of the Alb-AC mouse livers were lower than that of WT mice, even after normalizing to body weight (Fig. 2A**, right**). Histologically, the Alb-AC liver exhibited substantially less lipid accumulation compared to that of the WT control (Fig. 2B**, left**). Mirroring the histological findings, Alb-AC mice exhibited almost a three-fold decrease in hepatic triglyceride (TG) content compared to WT mice (Fig. 2B**, right**).

In addition, we performed a triglyceride clearance test by gavaging a lipid emulsion (20% Intralipid) to both Alb-AC and WT mice. Surprisingly, the Alb-AC mice peaked at higher levels and had a lower rate of triglyceride clearance compared to WT (Fig. 2C). To determine whether AC overexpression affected hepatic VLDL production, mice were fasted for 3 hours followed by intravenous injection of tyloxapol, a potent inhibitor of capillary lipoprotein lipase. Alb-AC mice had higher plasma TG levels compared to WT mice two hours post-injection, indicating that the rate of VLDL production in Alb-AC mice is markedly higher compared to WT mice (Fig. 2D).

We intravenously injected a ^{3}H-triolein tracer into Alb-AC and WT mice which allows for assessments of lipid storage and β oxidation rates in different tissues. Alb-AC mice have a reduced lipid uptake in the liver compared to WT mice; concurrent increases were observed in the gonadal and brown fat pads (Fig. 2E). Lipid oxidation was not significantly altered

(Supplemental Fig. 2A). In order to determine how overexpression of AC ameliorates hepatic steatosis, we performed microarray analyses on liver tissues specifically at 2 weeks post induction and then at 2 months post induction of the AC transgene in the *liver*. A *reduction* of genes in fatty acid (FA) synthesis and uptake pathways was evident. Quantitative PCR analyses confirmed the reduction in FA synthesis genes (ACC, FAS, Scd-1, Elolv5, and SREBP-1a) and FA uptake genes (CD36, FATP2, FATP5, L-FABP) by the end of week 8 (Supplemental Fig. 2B & C). Surprisingly, qPCR of the fatty acid synthesis genes and fatty acid uptake genes in *gWAT* showed a corresponding *increase* during this same period (Supplemental Fig. 2B & C).

A noticeable observation was the differences in fat pad distribution in Alb-AC mice compared to WTs when challenged with HFD-dox. Alb-AC gWAT was substantially larger than the corresponding pads in WT's after HFD-dox challenge when normalized to body weight, while the mWAT of Alb-AC was relatively smaller than its counterpart in WT littermates (Supplemental Fig. 2D & E). Furthermore, whole body NMR data shows that the overall composition of fat and lean mass in Alb-AC and WT mice are comparable (Supplemental Fig. 2F), thus suggesting that changes in fat pad weights are the result of redistribution rather than an overall increase or decrease of overall adipose tissue mass.

We evaluated gonadal adipose tissue for histological differences (Fig. 2F). While WT mice on HFD-dox displayed crown-like structures characteristic of immune infiltration, Alb-AC fat pads showed far fewer signs of inflammation. Mac-2 immunohistochemistry staining confirmed that Alb-AC fat pads had greatly reduced levels of infiltrated macrophages compared to those of WT. In addition, we found markedly less fibrosis in the fat pads of Alb-AC compared to their WT counterparts, as determined by trichrome staining (Fig. 2F). Expression of inflammatory cytokines such as TNF-α, IL-6, and IL-10 were substantially reduced in the gWAT of Alb-AC mice (Supplemental Fig. 2G). Furthermore, fibrosis markers such as Col1α, Col3α, and Col6α1 were also lower in the gWAT of Alb-AC mice compared to WT (Supplemental Fig. 2H). We examined the levels of ceramides in the gWAT of HFD-dox-fed Alb-AC and WT mice and found that dihydro-ceramides and hexosyl-ceramide species to be significantly lowered in Alb-AC mice after HFD-dox challenge compared to WT controls, while other ceramide species remained unaltered (Fig. 2G). Furthermore, there are no significant alterations in specific chain lengths of gWAT ceramides (Supplemental Fig. 2I). gWAT sphingoid species levels, especially sphingosine and sphinganine, were also significantly lowered in Alb-AC mice compared to WT (Fig. 2H). Ceramide synthesis pathway genes (SPT2, SK1, CerS6) were found to be significantly *reduced* in the *gWAT* of Alb-AC mice compared to WT at the end of 8 weeks of HFD-dox feeding (Supplemental Fig. 2J). By contrast, examination by qPCR of the genes in the ceramide synthesis pathway in the Alb-AC *liver* showed a profound *increase* in several ceramide synthase (CerS) genes including CerS2, CerS5, and CerS6. In contrast, CerS1 expression was significantly reduced (Supplemental Fig. 2J).

Acid Ceramidase Overexpression in White Adipose Tissue Improves Glucose Metabolism

By crossing the Tet-responsive acid ceramidase transgenic line (TRE-AC) with an **a**diponectin-**r**t**T**A transgenic allele (Art) we were able to achieve inducible overexpression

of acid ceramidase (Art-AC) within multiple WAT depots (Supplemental Fig. 3A). Upon doxycycline induction, AC overexpression is achieved exclusively in the fat pads and remains unchanged in other tissues, such as the liver (Supplemental Fig. 3B). In the absence of doxycycline, overexpression was not detected, but acid ceramidase expression rose 3.5-fold following exposure to doxycycline in the diet (200 mg/kg, 10 days, Supplemental Fig. 3C). This corresponded to a 1.8, 1.3, and 3.7-fold increase in acid ceramidase activity in sWAT, gWAT, and mWAT respectively, without alterations in hepatic ceramidase activity (Supplemental Fig. 3D). Furthermore, serum ceramidase activity in WT and Art-AC were not significantly altered (Supplemental Fig. 3E). The lack of ceramide hydrolysis was further confirmed with C17 ceramide, showing no alterations in hepatic ceramidase activity (Supplemental Fig. 3F). On a doxycycline-enriched chow diet, several ceramide subspecies were significantly reduced in mWAT, while total ceramides were significantly decreased in the liver (Supplemental Fig. 3G & H). Concomitant decreases in fasting glucose and glucose excursion during oral glucose tolerance tests were evident (Supplemental Fig. 3I) without any changes in body weight (34.4±3.1 versus 32.7±3.3 for wildtype and Art-AC, respectively).

Art-AC transgenic mice have a marked ability to maintain normal glucose homeostasis on high fat diet. Total ceramides were reduced in mesenteric (67%), gonadal (40%) and subcutaneous (30%) fat pads, with C16 and C18 ceramides showing the most consistent and robust changes (Fig. 3A). Serum sphingolipid species were also altered (Fig. 3B). Specifically, serum levels of $C_{20:0}$ ceramides were reduced to 42% of WT levels (Supplemental Fig. 3J). Glucose levels were lower during the fasted state and following an oral glucose challenge (Fig. 3C), while insulin levels remained markedly lower during fasting and 15 minutes following glucose administration (Fig. 3D). Improvements in insulin sensitivity were confirmed by the enhanced lowering of glucose upon insulin administration (Fig. 3E) and occurred without changes in body weight (40.0±5.0 versus 38.4±6.1 for wildtype and Art-AC, respectively). The improvements in whole-body glucose homeostasis and insulin sensitivity could hardly be explained by the relatively minor contribution of adipose to glucose disposal. To address this more specifically, we performed hyperinsulinemic-euglycemic clamps. The glucose infusion rate required to maintain euglycemia was markedly higher in Art-AC transgenic mice, confirming improvements in whole body insulin sensitivity (Fig. 3F). The kinetics of ^{3}H-glucose disposal were not altered, suggesting negligible changes in insulin stimulated glucose disposal by muscle (Supplemental Fig. 3K). Rather, Art-AC transgenic mice showed improvements in the ability of insulin to suppress endogenous glucose production (Fig. 3G). Specifically, endogenous glucose production was suppressed by ~60% in Art-AC compared to ~15% in WT (Supplemental 3L). These improvements in insulin sensitivity could not be explained by changes in body weight, circulating insulin during the clamped state, or variations in the achieved glucose concentrations during the clamped state (Table 1). Furthermore, there were no significant changes in lipolysis between WT and Art-AC mice under clamped or insulinopenic conditions (Table 1, Supplemental Fig. 3M). Enhanced insulin-stimulated phosphorylation of Akt was present in livers of these mice 30-minutes after insulin stimulation (Fig. 3H). Lowering ceramides in adipose also enhanced insulin-stimulated phosphorylation of Akt in gonadal fat pads, while changes in total Akt expression were not

altered in either tissue (Fig. 3H). The rate of 2-deoxyglucose uptake doubled in gonadal, mesenteric and subcutaneous fat of Art-AC transgenic mice (Fig. 3I).

Acid Ceramidase Overexpression in White Adipose Tissue Improves Hepatic Lipid Accumulation

We evaluated gonadal adipose tissue for histological differences (Fig. 4A). While WT mice on HFD-dox displayed crown-like structures characteristic of immune infiltration, Art-AC fat pads showed far fewer signs of inflammation. Mac-2 immunohistochemistry staining confirmed that Art-AC fat pads had greatly reduced levels of infiltrated macrophages compared to those of WT. In addition, we found markedly less fibrosis in the fat pads of Art-AC compared to their WT counterparts, as determined by trichrome staining (Fig. 4A). Correspondingly, mRNA levels of TNF-α and pro-fibrotic genes (Col1α1, Col3α1, Col6α1) were found to be notably lowered in WAT compared to WT (Supplemental Fig. 4A)

Considering the fact that overexpression of AC in the *liver* resulted in improvements in *adipose* tissue metabolic health, we wanted to examine if the reverse is also true. Dissection of the livers of the Art-AC transgenic mice clearly revealed less steatotic livers, judged by both overall appearance and color (Fig 4B**, left**). Hepatomegaly caused by a high fat diet is diminished by transgene overexpression in adipose tissue (Fig 4B**, right**). Lowering of hepatic triglyceride content was also evident histologically (Fig. 4C**, left**). Transgene overexpression in adipose tissue decreased hepatic triglyceride accumulation on chow diet by 45% (Supplemental Fig. 4B) and caused a 57% decrease in hepatic triglyceride while on high-fat diet (Fig. 4C**, right**).

We subsequently evaluated lipid metabolism in more detail. Neither fatty acids (Table 1) nor serum triglycerides (Fig. 4D) were different during the basal state. During hyperinsulinemic clamps, Art-AC mice showed a trend toward improved suppression of lipolysis ($p=0.06$), as serum fatty acids trended lower in Art-AC transgenic mice during the clamped state (Table 1). By contrast, no changes in glycerol were apparent in the clamped state. Following lipid gavage, the triglyceride clearance was not different between WT and Art-AC transgenic mice (Fig. 4D). Hepatic secretion of triglyceride was not affected by adipose-restricted expression of acid ceramidase (Fig 4E). In a complimentary approach, uptake of tritiated oleate was not significantly altered in any of the fat pads evaluated following an intravenous bolus of ^{3}H-Triolein (Fig. 4F). Lipid oxidation was not altered in any of the tissues evaluated (Supplemental Fig. 4C). Unlike adipose tissues, livers of transgenic mice displayed a 3.8-fold decrease in lipid uptake (Fig. 4F). Furthermore, levels of C16:0 and C18:0 ceramide species were also markedly lower in Art-AC compared to WT (Fig. 4G). Hepatic diacylglycerols were not significantly altered (Supplemental Fig. 4D).

Adipose-specific ceramidase reverses insulin resistance and hepatic steatosis more rapidly than liver-specific ceramidase induction

To determine whether the induction of AC in the liver or adipose is able to *reverse* impairments in total body glucose metabolism and *rescue* hepatic steatosis, Alb-AC, Art-AC, and WT mice were first fed a doxycycline-free HFD for 2 months to facilitate the development of hepatic steatosis prior to transgene induction. At the end of the 2 months,

diets were switched to HFD-dox to induce AC overexpression. Approximately one month after transgene induction in the *liver*, we found $C_{16:0}$ and $C_{18:0}$ ceramide levels to be appreciably lowered along with concurrent improvements in insulin signaling, as indicated by increased phosphorylation of Akt (Fig. 5A & B). Furthermore, hepatic lipid accumulation was significantly lowered 4-weeks after inducing overexpression of the transgene in the liver (Fig. 5C). An insulin tolerance test does not reveal any changes 3 days post induction of AC in the liver (Fig. 5D). Our data not only showed that the effects of the transgene take about one month to result in significant physiological effects, but also that the local overexpression of AC in the liver can rescue livers with severe steatosis *after* the steatosis has fully developed.

Overexpression of AC within the adipocyte offers a much more rapid rescue of insulin resistance and hepatic steatosis. C16 and C18 hepatic ceramides are substantially decreased within 3 days of treatment (Fig. 5E). Western blotting for p-Akt in the liver of Art-AC mice shows improvements in p-Akt levels upon insulin administration within as short as three days post induction of AC (Fig. 5F). Within 3 days of transgene activation in the adipocyte, hepatic triglyceride content is lower and continues to improve substantially throughout the 4-week doxycycline treatment (Fig. 5G). Remarkably, insulin-stimulated lowering of blood glucose is improved compared to wildtype littermates during insulin tolerance tests after just 3 days (Fig. 5H). Collectively, these data show the ability of ceramidase to overcome previously established metabolic perturbations promoted by diet-induced obesity, with slightly different kinetics depending on whether we express AC in hepatocytes or in adipocytes.

Ceramides influence hepatic lipid uptake via PKCζ-mediated influence on CD36, and AC downregulates lipid uptake and fatty acid synthesis genes in the liver

Livers from Alb-AC and Art-AC mice showed comparable decreases in expression of CD36 as compared to WT littermates (Fig. 6A). The relative abundance of hepatic CD36 protein was also clearly reduced in both Art-AC and Alb-AC transgenic mice (Fig. 6B).

In addition to their roles as mediators of ceramide-induced insulin resistance, atypical PKCs have been noted to relay critical signals for lipogenesis and lipid uptake (Luiken et al., 2009; Sajan et al., 2004; Sajan et al., 2009; Taniguchi et al., 2006). Consistent with this, aPKC expression (Fig. 6C) and activity (Fig. 6D) were decreased in the livers of Alb-AC and Art-AC transgenic mice. Furthermore, aPKC activity was significantly lowered in Art-AC mice after only three days of doxycycline treatment (Supplemental Fig. 5A).

Since aPKCs can play a permissive role in CD36 translocation, we evaluated the propensity for ceramide to facilitate lipid uptake. In cultured H4IIe hepatocyte cells, a 1 hour pre-incubation with the short chain ceramide analog C2-ceramide was sufficient to stimulate a 63% increase in palmitate uptake (Fig. 6E) and markedly enhanced aPKC activity (Fig. 6F). Incubation of cells with C2-ceramide yielded the same lipid uptake results as when cells were pretreated with palmitate, which promotes the formation of endogenous ceramides intracellularly (Supplemental Fig. 5B). To evaluate the requirement for aPKC in this effect, we blocked aPKC activation by including a myristoylated PKCζ pseudosubstrate inhibitor which completely prevented ceramide-induced lipid uptake, as it prevented ceramide from

activating PKCζ (Fig. 6E and F). To confirm this genetically, we achieved overexpression of dominant negative (dn)PKCζ or expression of constitutively active (ca)PKCζ via transient transfection. Following overexpression with dnPKCζ, C2-ceramide failed to stimulate PKCζ activity in cells expressing dnPKCζ, and it also failed to stimulate lipid uptake. By contrast, overexpression of (ca)PKCζ stimulated PKCζ activity to the same degree as C2-ceramide, and was sufficient to increase palmitate uptake, but could not be further enhanced by ceramide addition (Fig. 6E and F). Immunohistological staining of H4IIe cells grown in glass bottom culture dishes showed that treatment with C2-ceramide resulted in both an increase in CD36 translocation to the membrane as judged by an increase in plasma membrane localized intensity of CD36 signal compared to cells treated with DMSO (Fig. 6G). Following overexpression with dnPKCζ, C2-ceramide failed to stimulate CD36 translocation to the membrane, as there is no change between plasma membrane localized intensity of CD36 signal between C2-ceramide and DMSO treated cells (Fig. 6G). Conversely, overexpression of (ca)PKCζ in H4IIe cells resulted in an increase in CD36 translocation to the membrane, treatment with C2-ceramide of the (ca)PKCζ transfected cells did not increase the signal intensity of CD36 in the plasma membrane (Fig. 6G). As sphingosine, a byproduct of the ceramidase reaction is a known inhibitor of multiple PKCs we also evaluated the propensity for sphingosine to alter aPKC activation and lipid uptake. Incubation of H4IIe cells with sphingosine, rather than ceramide impaired aPKC activity (Supplemental Fig. 5C) and diminished palmitate uptake (Supplemental Fig. 5D).

To confirm our findings *in vivo*, we first induced hepatic steatosis in Alb-AC and Art-AC mice and their littermate controls with four weeks of HFD feeding. We subsequently injected both the transgenic and WT mice with either PBS or 2-acetyl-1,3-cyclopentanedione (ACPD), a known PKCζ inhibitor demonstrated in previous studies to effectively reduce PKCζ activity (Sajan et al., 2014b), and compared the results with WT and transgenic mice fed a doxycycline diet. For the Alb-AC cohort, we found that injection of ACPD for one month in WT and Alb-AC mice resulted in the same improvements in insulin sensitivity and reduction in hepatic lipid accumulation as Alb-AC mice fed a HFD-dox diet for the same time (Fig. 6H and I). Similarly, injection of ACPD in Art-AC and WT mice resulted in a more rapid improvement in insulin sensitivity and hepatic lipid accumulation after three days of injection, mimicking the effects of three days of HFD-dox diet in Art-AC mice (Fig. 6H and I).

Discussion

Here, we report the first mouse models demonstrating inducible decreases of ceramide within the liver and adipose. The use of an adiponectin promoter-driven rtTA (Art) has allowed us to evaluate the adipocyte-specific contributions of sphingolipids to whole-body metabolic dysfunction for the first time. Our inducible acid ceramidase model bypasses the compensatory mechanisms and developmental issues present in constitutive models, and gives us the opportunity to study acute modifications of ceramide-induced metabolic dysfunction in adult mice. With this system, we demonstrate that the acute depletion of ceramide in hepatocytes or adipocytes of adult mice can prevent and reverse the development of hepatic steatosis while simultaneously improving systemic glucose tolerance and insulin sensitivity in adult mice with diet-induced obesity. These studies highlight the

prominent cross-talk between the liver and adipose tissue that allows for equilibration of sphingolipids between the two tissues. Furthermore, these studies are the first to define a causal role for ceramide in the pathogenesis of diet-induced NAFLD.

We found that that C16:0 and $C_{18:0}$ ceramide levels to be 50% of WT in Alb-AC mice livers, indicating that the hepatic accumulation of particular ceramide subspecies more prominently contributes to the development of NAFLD and systemic insulin resistance. Consistent with our findings, recent work has shown that mice with ceramide synthase 6 deficiency ($cerS6^{\Delta/\Delta}$) exhibit reduced C16:0 ceramide levels and are protected from high fat diet-induced obesity and glucose intolerance (Turpin et al., 2014). By contrast, heterozygous deletion of ceramide synthase 2 promotes a paradoxical increase in C16:0 ceramides to confer greater susceptibility to diet induced insulin resistance (Raichur et al., 2014). Importantly, we also observed that concurrent with the lowering of hepatic ceramides, hepatic DAG levels were *increased* in our Alb-AC mice to almost double of those measured in WT mice. In line with several studies, these findings further question the role of liver DAGs as a causative agent of hepatic steatosis and insulin resistance (Brown et al., 2010; Farese et al., 2012; Minehira et al., 2008; Monetti et al., 2007; Voshol et al., 2003). Nonetheless, this does not rule out the possibility that a particular DAG subspecies (i.e. sn-1,2-diacylglyerols) is able to induce hepatic steatosis and insulin resistance under certain conditions (Boni and Rando, 1985). Thus, these studies directly link excess accumulation of hepatic ceramide to the development of non-alcoholic fatty liver disease and systemic insulin resistance in rodents.

Elevated circulating ceramides are observed in patients with type 2 diabetes and these levels correlate with the severity of insulin resistance (Boon et al., 2013; Haus et al., 2009; Lopez et al., 2013). Whether plasma ceramides are a contributor or merely a marker of systemic insulin resistance has been unresolved. We show that when ceramide species are acutely broken down in liver and adipose of obese mice, there is also a corresponding significant lowering of plasma ceramides. Thus, our current findings not only suggest that the liver can be a major contributor of circulating ceramide species, but also reveal that the adipocyte may also contribute substantially to changes in serum ceramides. While it appears likely that these two tissues shuttle a common pool of sphingolipids back and forth through the circulation, it remains uncertain if the adipose supplies the liver with ceramides- where they can be repackaged into lipoprotein particles. Alternatively, each of these tissues may function as a sink whereby excess circulating ceramides may be taken up from the circulation for storage or metabolism. Furthermore, these findings point to the notion that plasma ceramide levels reflect changes in hepatic ceramide levels and are valuable markers of hepatic metabolic health.

The roles of atypical PKCs as mediators of ceramide-induced insulin resistance have been previously reported. In particular, C16 ceramides are potent activators of PKCζ activity *in vitro* (Muller et al., 1995). Specifically, in cultured muscle cell lines PKCζ can phosphorylate the plextrin homology domain of Akt on threonine residue 34 (Powell et al., 2003). This phosphorylation site alters the affinity for Akt to 3,4,5-trisphosphate, thus interfering with Akt translocation to plasma membrane microdomains where it is activated (Fox et al., 2007). A recent report by the Farese group suggests that aberrant activation of

atypical PKC, is evident in livers of $Lep^{ob/ob}$ mice and is essential for impairments in Akt mediated signaling to FoxO1; this is rescued *in vivo* by pharmacological inhibition of atypical PKCs (Sajan et al., 2014b). PKCζ has also attracted attention for its role in lipid homeostasis, particularly as a mediator of SREBP-1c driven lipogenesis (Sajan et al., 2004; Sajan et al., 2009; Taniguchi et al., 2006). Moreover, PKCζ has also been previously noted to play a facilitative role in CD36 activation to promote lipid uptake into cardiomyocytes (Luiken et al., 2009). We show here that targeted manipulation of ceramide alters atypical PKC activation in the liver. As such, our data support the notion that ceramides may be a causal effector of selective insulin resistance by driving atypical PKC activation and associated lipogenic and lipid uptake processes, while simultaneously impairing Akt-mediated regulation of hepatic glucose output. The contribution of sphingoid bases to this process is intriguing, as sphingosine can stimulate or suppress PKCζ activation, depending on the dosage (Muller et al., 1995). Here, we note the potential of sphingosine to impair the activation of aPKC and prevent lipid uptake. The rapid release of sphingosine from the adipocyte into the portal circulation for delivery to the liver may explain how adipose-specific ceramidase activation exerts more rapid beneficial effects on the liver.

Collectively, our data suggest that the accumulation of ceramides is critical in the development of non-alcoholic fatty liver disease and hepatic insulin resistance. Induction of AC activity rescues existing hepatic steatosis and metabolic syndrome in mice with diet induced obesity, suggesting that it is a potential therapeutic target. Strategies for AC enzyme replacement have been under development for the treatment of Farber Disease (AC deficiency) (Schuchman and Galanin, 2014), and this may provide additional benefits in the form of systemic metabolic improvements. Past clinical data has shown that serum adiponectin levels inversely correlate with hepatic triglyceride content (Turer et al., 2012). Considering that adiponectin's main target tissue is the liver and it is known to confer ceramidase activity through its receptors AdipoR1 and R2, we expect adiponectin to exert similar effects as seen for our acid ceramidase transgene, such as reducing hepatic triglyceride accumulation and improving hepatic insulin sensitivity (Holland et al., 2011).

Methods and Materials

Animals

All animal experimental protocols were approved by the Institutional Animal Care and Use Committee of University of Texas Southwestern Medical Center at Dallas. TRE-AC mice were generated by subcloning the mouse AC gene into a plasmid containing the TetO element. Following linearization, the construct was injected into C57/Bl6-derived blastocysts. Transgene-positive offspring were genotyped using PCR with the following primer sets: TRE-AC, 5′-GACTGTATTCACAACCTTGATG and 5′-CATCTTCCCATTCTAAACAAC.

The *Rosa26-loxP-stop-loxP-rtTA* and *Albumin-Cre* mice were lines were obtained from Jackson Laboratories. *Albumin-Cre* mice were bred with the *Rosa26-loxP-stop-loxP-rtTA* mice to achieve liver-specific expression of rtTA. This mouse was subsequently crossed to the TRE-AC transgenic mice. The resulting triple transgenic mice expressed AC in liver only after exposure to doxycycline (Dox). All overexpression experiments were performed

in a pure C57/Bl6 background. All experiments were conducted using littermate-controlled male mice. All Dox-chow diet (200 mg/kg Dox) or HFD-Dox (200 mg/kg Dox) experiments were initiated at approximately 6-16 weeks of age.

Acid ceramidase activity assay

Acid ceramidase activity was determined by a fluorimetric assay using the substrate Rbm 14-12, a synthetic ceramide analog that possess a 12-carbon fatty acid chain length, at 20 uM after incubation for 3 hours with tissue lysates (20 ug protein) of both wild-type mice (WT) and Alb-AC mice after 8 weeks of HFD-dox (Bedia et al., 2010).

Lipid quantifications

Sphingolipids were quantified as described previously by LC/ESI/MS/MS using a Shimadzu Nexera X2 UHPLC system coupled to a Shimadzu LCMS-8050 triple quadrupole mass spectrometer (Holland et al., 2011). Diacylglycerol and C17 FFA were quantified using an ABI 5600+ (AB Sciex) following direct infusion of extracted lipids containing 18 mM ammonium fluoride to aid in ionization of neutrals and to reduce salt adducts. Data from the AB Sciex 5600+ was collected and calibrated with Analyst and PeakView Software (AB Sciex, Framingham, MA). Lipid species were identified based on exact mass and fragmentation patterns, and verified by lipid standards.

Streptozotocin (STZ) administration

Mice were fasted for 6 hrs and subjected to a single i.p. injection of streptozotocin (STZ, Sigma #S1030, St. Louis, MO) at the dose of 135 ug/g BDW. STZ was stored at −20 °C as powder, and freshly diluted in ice-cold sodiu m citrate buffer (0.1M, pH 4.5) before injection as previously described (Ye et al., 2014).

aPKC inhibitor

Inhibitor of aPKCs, PKC-I and PKC-ζ, 2-acetyl-1,3-cyclopentanedione (ACPD), was purchased from Sigma (St. Louis, MO). Its specificity was reported previously (Sajan et al., 2014a). In addition, we presently found that ACPD did not inhibit kinases, Akt2, FGFR1/2/3/4, mTOR, GSK3β, IRAK1/4, JAK1/2, MEK1, ERK1/2, JNK1/2, PKA, Src, ROCK2, ROS1, or PI3Kα/α, as tested by Life Technologies (Madison WI). Alb-AC and WT controls were injected subcutaneously daily with ACPD (10 mg/kg) in PBS or PBS only for one month. Art-AC and WT controls were injected subcutaneously daily with ACPD (10 mg/kg) in PBS or PBS only for 3 days.

Cell culture

H4IIe rat hepatoma cells were cultured in low glucose DMEM supplemented with 10% fetal bovine serum. Dominant negative PKCζ (Soh and Weinstein, 2003)and caPKCζ (Chou et al., 1998) were purchased from Addgene (Cambridge MA) and transfections were performed with lipofectamine 3000 (Invitrogen, Grand Island NY) according to the manufacturer’s instructions

Statistics

All results are provided as means ± s.e.m. All statistical analyses were performed using GraphPad Prism. Differences between the two groups over time (indicated in the relevant figure legends) were determined by a two-way analysis of variance for repeated measures. For comparisons between two independent groups, a Student's *t* test was used. Significance was accepted at $P < 0.05$.

Supplementary Material

Refer to Web version on PubMed Central for supplementary material.

Acknowledgements

We thank Dr. Bob Hammer and the Transgenic Core Facility at UTSW for the generation of the transgenic lines, John Shelton and the Histology Core for assistance with histology and the UTSW Metabolic Core Unit for help in phenotyping. We would also like to thank Shimadzu Scientific Instruments for the collaborative effort and the expert advice on the mass spec instrumentation side. Supported by the National Institutes of Health (grants R01-DK55758, R01-DK099110 and P01DK088761-01 to PES). JYX is supported by a NIH fellowship 1F30-DK100095. WLH is supported by a K99-DK094973, JDRF Award 5-CDA-2014-185-A-N, and an AHA Beginning Grant in Aid 12BGI-A8910006.

References

Bedia C, Camacho L, Abad JL, Fabrias G, Levade T. A simple fluorogenic method for determination of acid ceramidase activity and diagnosis of Farber disease. Journal of lipid research. 2010; 51:3542–3547. [PubMed: 20871013]

Bektas M, Allende ML, Lee BG, Chen W, Amar MJ, Remaley AT, Saba JD, Proia RL. Sphingosine 1-phosphate lyase deficiency disrupts lipid homeostasis in liver. The Journal of biological chemistry. 2010; 285:10880–10889. [PubMed: 20097939]

Birkenfeld AL, Shulman GI. Nonalcoholic fatty liver disease, hepatic insulin resistance, and type 2 diabetes. Hepatology. 2014; 59:713–723. [PubMed: 23929732]

Boni LT, Rando RR. The nature of protein kinase C activation by physically defined phospholipid vesicles and diacylglycerols. The Journal of biological chemistry. 1985; 260:10819–10825. [PubMed: 3161882]

Boon J, Hoy AJ, Stark R, Brown RD, Meex RC, Henstridge DC, Schenk S, Meikle PJ, Horowitz JF, Kingwell BA, et al. Ceramides contained in LDL are elevated in type 2 diabetes and promote inflammation and skeletal muscle insulin resistance. Diabetes. 2013; 62:401–410. [PubMed: 23139352]

Brown JM, Betters JL, Lord C, Ma Y, Han X, Yang K, Alger HM, Melchior J, Sawyer J, Shah R, et al. CGI-58 knockdown in mice causes hepatic steatosis but prevents diet-induced obesity and glucose intolerance. Journal of lipid research. 2010; 51:3306–3315. [PubMed: 20802159]

Chavez JA, Knotts TA, Wang LP, Li G, Dobrowsky RT, Florant GL, Summers SA. A role for ceramide, but not diacylglycerol, in the antagonism of insulin signal transduction by saturated fatty acids. The Journal of biological chemistry. 2003; 278:10297–10303. [PubMed: 12525490]

Chou MM, Hou W, Johnson J, Graham LK, Lee MH, Chen CS, Newton AC, Schaffhausen BS, Toker A. Regulation of protein kinase C zeta by PI 3-kinase and PDK-1. Current biology : CB. 1998; 8:1069–1077. [PubMed: 9768361]

Farese RV Jr. Zechner R, Newgard CB, Walther TC. The problem of establishing relationships between hepatic steatosis and hepatic insulin resistance. Cell metabolism. 2012; 15:570–573. [PubMed: 22560209]

Fox TE, Houck KL, O'Neill SM, Nagarajan M, Stover TC, Pomianowski PT, Unal O, Yun JK, Naides SJ, Kester M. Ceramide recruits and activates protein kinase C zeta (PKC zeta) within structured

membrane microdomains. The Journal of biological chemistry. 2007; 282:12450–12457. [PubMed: 17308302]

Haus JM, Kashyap SR, Kasumov T, Zhang R, Kelly KR, Defronzo RA, Kirwan JP. Plasma ceramides are elevated in obese subjects with type 2 diabetes and correlate with the severity of insulin resistance. Diabetes. 2009; 58:337–343. [PubMed: 19008343]

Holland WL, Brozinick JT, Wang LP, Hawkins ED, Sargent KM, Liu Y, Narra K, Hoehn KL, Knotts TA, Siesky A, et al. Inhibition of ceramide synthesis ameliorates glucocorticoid-, saturated-fat-, and obesity-induced insulin resistance. Cell metabolism. 2007; 5:167–179. [PubMed: 17339025]

Holland WL, Miller RA, Wang ZV, Sun K, Barth BM, Bui HH, Davis KE, Bikman BT, Halberg N, Rutkowski JM, et al. Receptor-mediated activation of ceramidase activity initiates the pleiotropic actions of adiponectin. Nature medicine. 2011; 17:55–63.

Hoy AJ, Bruce CR, Turpin SM, Morris AJ, Febbraio MA, Watt MJ. Adipose triglyceride lipase-null mice are resistant to high-fat diet-induced insulin resistance despite reduced energy expenditure and ectopic lipid accumulation. Endocrinology. 2011; 152:48–58. [PubMed: 21106876]

Ichi I, Nakahara K, Fujii K, Iida C, Miyashita Y, Kojo S. Increase of ceramide in the liver and plasma after carbon tetrachloride intoxication in the rat. Journal of nutritional science and vitaminology. 2007; 53:53–56. [PubMed: 17484380]

Lopez X, Goldfine AB, Holland WL, Gordillo R, Scherer PE. Plasma ceramides are elevated in female children and adolescents with type 2 diabetes. Journal of pediatric endocrinology & metabolism : JPEM. 2013; 26:995–998. [PubMed: 23612696]

Luiken JJ, Ouwens DM, Habets DD, van der Zon GC, Coumans WA, Schwenk RW, Bonen A, Glatz JF. Permissive action of protein kinase C-zeta in insulin-induced CD36- and GLUT4 translocation in cardiac myocytes. The Journal of endocrinology. 2009; 201:199–209. [PubMed: 19273501]

Minehira K, Young SG, Villanueva CJ, Yetukuri L, Oresic M, Hellerstein MK, Farese RV Jr. Horton JD, Preitner F, Thorens B, et al. Blocking VLDL secretion causes hepatic steatosis but does not affect peripheral lipid stores or insulin sensitivity in mice. Journal of lipid research. 2008; 49:2038–2044. [PubMed: 18515909]

Monetti M, Levin MC, Watt MJ, Sajan MP, Marmor S, Hubbard BK, Stevens RD, Bain JR, Newgard CB, Farese RV Sr. et al. Dissociation of hepatic steatosis and insulin resistance in mice overexpressing DGAT in the liver. Cell metabolism. 2007; 6:69–78. [PubMed: 17618857]

Monsenego J, Mansouri A, Akkaoui M, Lenoir V, Esnous C, Fauveau V, Tavernier V, Girard J, Prip-Buus C. Enhancing liver mitochondrial fatty acid oxidation capacity in obese mice improves insulin sensitivity independently of hepatic steatosis. Journal of hepatology. 2012; 56:632–639. [PubMed: 22037024]

Muller G, Ayoub M, Storz P, Rennecke J, Fabbro D, Pfizenmaier K. PKC zeta is a molecular switch in signal transduction of TNF-alpha, bifunctionally regulated by ceramide and arachidonic acid. The EMBO journal. 1995; 14:1961–1969. [PubMed: 7744003]

Okada-Iwabu M, Yamauchi T, Iwabu M, Honma T, Hamagami K, Matsuda K, Yamaguchi M, Tanabe H, Kimura-Someya T, Shirouzu M, et al. A small-molecule AdipoR agonist for type 2 diabetes and short life in obesity. Nature. 2013; 503:493–499. [PubMed: 24172895]

Powell DJ, Hajduch E, Kular G, Hundal HS. Ceramide disables 3-phosphoinositide binding to the pleckstrin homology domain of protein kinase B (PKB)/Akt by a PKCzeta-dependent mechanism. Molecular and cellular biology. 2003; 23:7794–7808. [PubMed: 14560023]

Raichur S, Wang ST, Chan PW, Li Y, Ching J, Chaurasia B, Dogra S, Ohman MK, Takeda K, Sugii S, et al. CerS2 Haploinsufficiency Inhibits beta-Oxidation and Confers Susceptibility to Diet-Induced Steatohepatitis and Insulin Resistance. Cell metabolism. 2014; 20:687–695. [PubMed: 25295789]

Sajan MP, Acevedo-Duncan ME, Standaert ML, Ivey RA, Lee M, Farese RV. Akt-dependent phosphorylation of hepatic FoxO1 is compartmentalized on a WD40/ProF scaffold and is selectively inhibited by aPKC in early phases of diet-induced obesity. Diabetes. 2014a; 63:2690–2701. [PubMed: 24705403]

Sajan MP, Ivey RA, Lee MC, Farese RV. Hepatic insulin resistance in ob/ob mice involves increases in ceramide, atypical PKC activity and selective impairment of Akt-dependent FoxO1 phosphorylation. Journal of lipid research. 2014b

Sajan MP, Standaert ML, Miura A, Kahn CR, Farese RV. Tissue-specific differences in activation of atypical protein kinase C and protein kinase B in muscle, liver, and adipocytes of insulin receptor substrate-1 knockout mice. Molecular endocrinology. 2004; 18:2513–2521. [PubMed: 15256535]

Sajan MP, Standaert ML, Rivas J, Miura A, Kanoh Y, Soto J, Taniguchi CM, Kahn CR, Farese RV. Role of atypical protein kinase C in activation of sterol regulatory element binding protein-1c and nuclear factor kappa B (NFkappaB) in liver of rodents used as a model of diabetes, and relationships to hyperlipidaemia and insulin resistance. Diabetologia. 2009; 52:1197–1207. [PubMed: 19357831]

Schuchman EH, Galanin I. Development of enzyme replacement therapy for Farber disease and other disorders with ceramide storage. Mol Genet Metab. 2014; 111:S94–S94.

Shimomura I, Bashmakov Y, Horton JD. Increased levels of nuclear SREBP-1c associated with fatty livers in two mouse models of diabetes mellitus. The Journal of biological chemistry. 1999a; 274:30028–30032. [PubMed: 10514488]

Shimomura I, Bashmakov Y, Ikemoto S, Horton JD, Brown MS, Goldstein JL. Insulin selectively increases SREBP-1c mRNA in the livers of rats with streptozotocin-induced diabetes. Proceedings of the National Academy of Sciences of the United States of America. 1999b; 96:13656–13661. [PubMed: 10570128]

Shulman GI. Ectopic fat in insulin resistance, dyslipidemia, and cardiometabolic disease. The New England journal of medicine. 2014; 371:1131–1141. [PubMed: 25229917]

Soh JW, Weinstein IB. Roles of specific isoforms of protein kinase C in the transcriptional control of cyclin D1 and related genes. The Journal of biological chemistry. 2003; 278:34709–34716. [PubMed: 12794082]

Taniguchi CM, Kondo T, Sajan M, Luo J, Bronson R, Asano T, Farese R, Cantley LC, Kahn CR. Divergent regulation of hepatic glucose and lipid metabolism by phosphoinositide 3-kinase via Akt and PKClambda/zeta. Cell metabolism. 2006; 3:343–353. [PubMed: 16679292]

Taniguchi CM, Ueki K, Kahn R. Complementary roles of IRS-1 and IRS-2 in the hepatic regulation of metabolism. The Journal of clinical investigation. 2005; 115:718–727. [PubMed: 15711641]

Turer AT, Browning JD, Ayers CR, Das SR, Khera A, Vega GL, Grundy SM, Scherer PE. Adiponectin as an independent predictor of the presence and degree of hepatic steatosis in the Dallas Heart Study. The Journal of clinical endocrinology and metabolism. 2012; 97:E982–986. [PubMed: 22438228]

Turpin SM, Nicholls HT, Willmes DM, Mourier A, Brodesser S, Wunderlich CM, Mauer J, Xu E, Hammerschmidt P, Bronneke HS, et al. Obesity-Induced CerS6-Dependent C16:0 Ceramide Production Promotes Weight Gain and Glucose Intolerance. Cell metabolism. 2014; 20:678–686. [PubMed: 25295788]

Voshol PJ, Haemmerle G, Ouwens DM, Zimmermann R, Zechner R, Teusink B, Maassen JA, Havekes LM, Romijn JA. Increased hepatic insulin sensitivity together with decreased hepatic triglyceride stores in hormone-sensitive lipase-deficient mice. Endocrinology. 2003; 144:3456–3462. [PubMed: 12865325]

Wiesner P, Leidl K, Boettcher A, Schmitz G, Liebisch G. Lipid profiling of FPLC-separated lipoprotein fractions by electrospray ionization tandem mass spectrometry. Journal of lipid research. 2009; 50:574–585. [PubMed: 18832345]

Xia JY, Morley TS, Scherer PE. The adipokine/ceramide axis: key aspects of insulin sensitization. Biochimie. 2014; 96:130–139. [PubMed: 23969158]

Ye R, Holland WL, Gordillo R, Wang M, Wang QA, Shao M, Morley TS, Gupta RK, Stahl A, Scherer PE. Adiponectin is essential for lipid homeostasis and survival under insulin deficiency and promotes beta-cell regeneration. eLife. 2014; 3

Yetukuri L, Katajamaa M, Medina-Gomez G, Seppanen-Laakso T, Vidal-Puig A, Oresic M. Bioinformatics strategies for lipidomics analysis: characterization of obesity related hepatic steatosis. BMC systems biology. 2007; 1:12. [PubMed: 17408502]

Yu XX, Murray SF, Pandey SK, Booten SL, Bao D, Song XZ, Kelly S, Chen S, McKay R, Monia BP, et al. Antisense oligonucleotide reduction of DGAT2 expression improves hepatic steatosis and hyperlipidemia in obese mice. Hepatology. 2005; 42:362–371. [PubMed: 16001399]

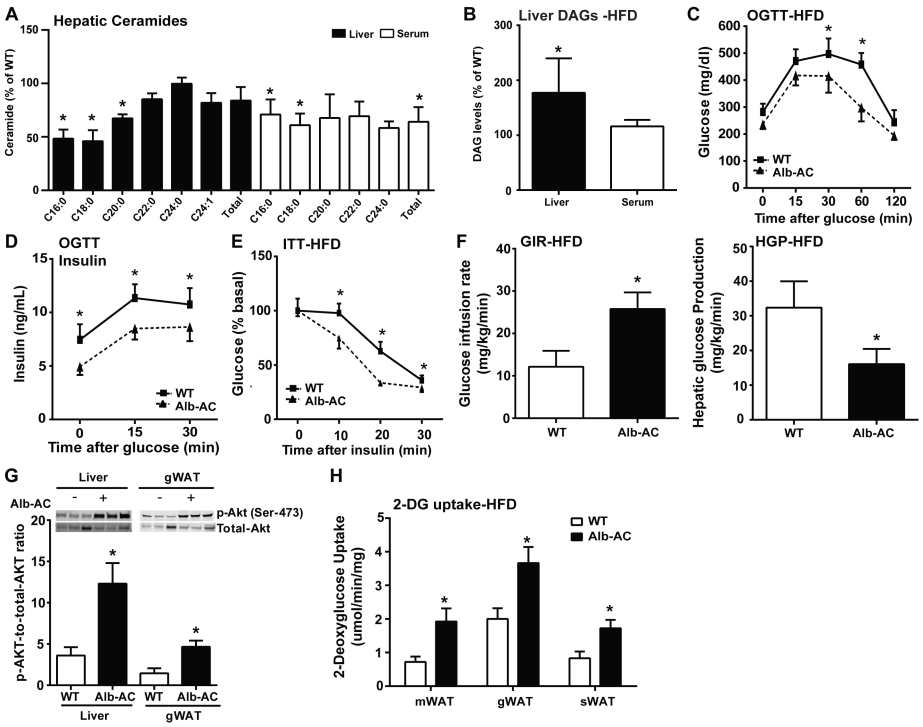

Fig. 1. Inducible liver-specific overexpression of acid ceramidase results in significantly reduced $C_{16:0}$ ceramide species in the liver and improved total body glucose homeostasis and insulin sensitivity under HFD feeding

A) Analysis of liver and serum ceramide species from Alb-AC mice and WT littermates. **B)** Analysis of liver and serum diacylglycerol (DAG) levels in Alb-AC mice and control littermates after. **C)** Circulating glucose levels were measured during an oral glucose tolerance test (OGTT) (2.5g/kg glucose per oral gavage). **D)** Serum insulin levels during the OGTT were quantified via ELISA. **E)** Circulating glucose levels measured during an insulin tolerance test (ITT) (0.75 U/kg). **F)** Glucose infusion rates (left) and hepatic glucose output (right) during hyperinsulinemic-euglycemic clamp experiments performed on conscious unrestrained 10-week-old WT and Alb-AC males. **G)** Representative immunoblots of phosphorylated and total Akt of insulin stimulated WT and Alb-AC mice, shown in triplicate. **H)** 2-deoxyglucose uptake quantification on conscious unrestrained 10-week-old WT mice and Alb-AC males. All samples are from Alb-AC mice and WT littermates after 8 weeks of HFD –dox challenge (n = 6), unless specified otherwise. **P*<0.05 by Student's *t* test.

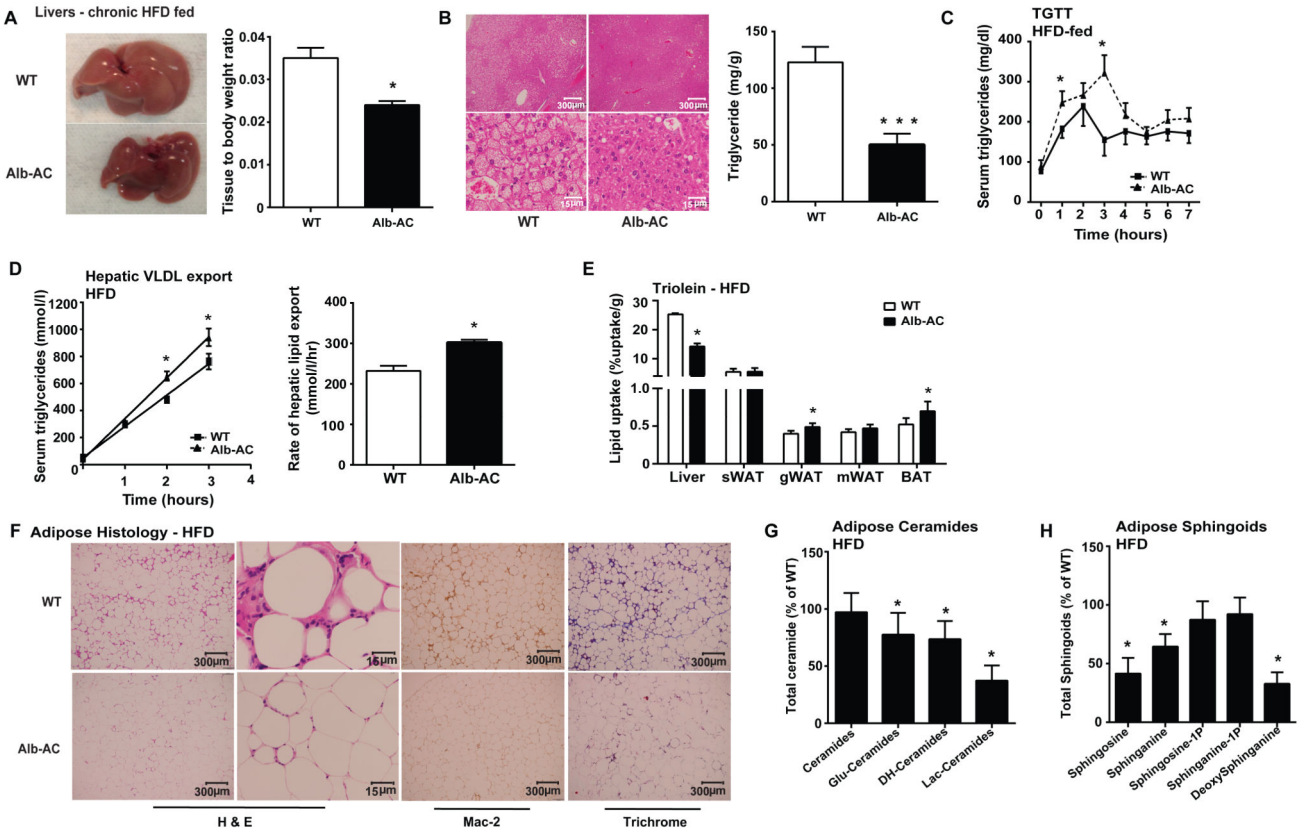

Fig. 2. Liver specific overexpression of acid ceramidase significantly reduces hepatic lipid accumulation and improves adipose tissue metabolic health when challenged with HFD

A) A representative gross image of WT and Alb-AC livers. Bar graphs on the right represent the mass of the liver normalized to the total body weight of the mice. **B)** Representative H&E stained images of WT and Alb-AC livers. Bar graphs on the right represent quantification of liver triglyceride levels. **C)** Circulating triglyceride (TG) levels were measured during an oral TG clearance test (20% intralipid, 15 uL/g body weight; single gavage) in Alb-AC mice and WT littermate controls. **D)** Circulating triglyceride levels and the rate of hepatic VLDL export were measured following intravenous injection of tyloxapol (500 mg/kg) to inhibit plasma VLDL clearance in Alb-AC mice and WT littermate controls. **E)** Total ^{3}H-triolein lipid-uptake per tissue in WT and Alb-AC males at 15 min after injection (2 Ci per mouse in 100 l of 5% intralipid, single tail-vein injection). **F)** Representative images of H&E, Mac-2, and trichrome staining of WT and Alb-AC gonadal fat pads. **G)** Total WAT ceramide species levels were quantified by tandem MS/MS. **H)** Total WAT sphingoid species levels were quantified by tandem MS/MS. All samples are from Alb-AC mice and WT littermates after 8 weeks of HFD–dox challenge (n = 6), unless specified otherwise. **P*<0.05, ****P*<0.001 by Student's *t* test.

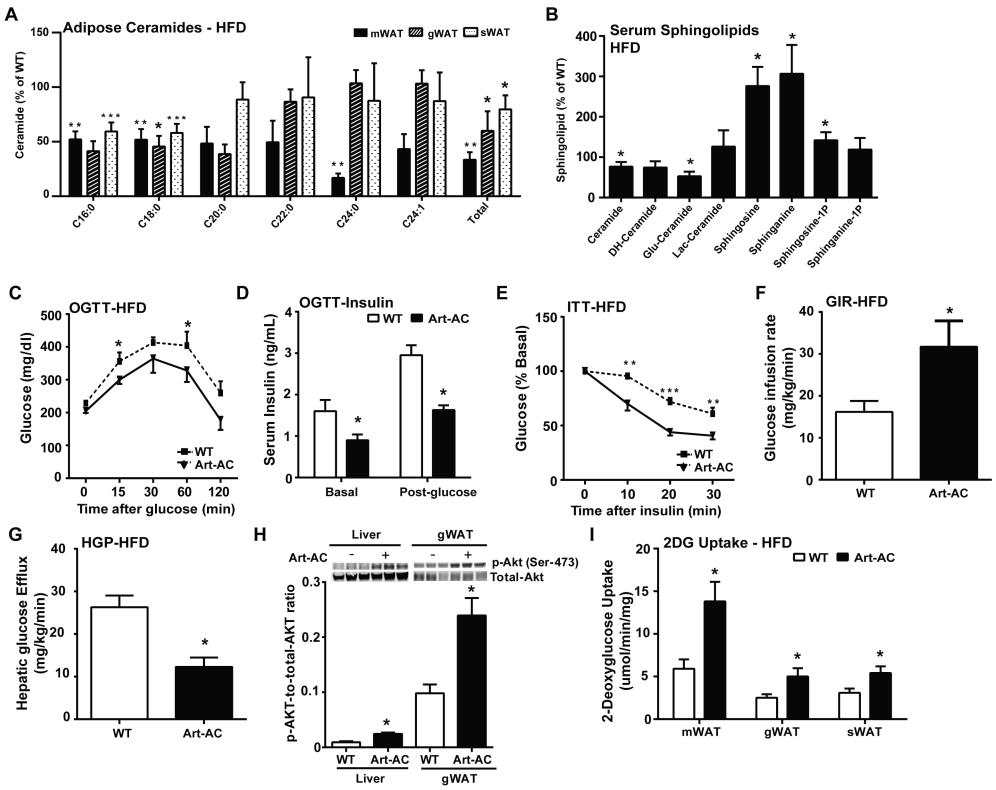

Fig. 3. Inducible adipose-specific overexpression of acid ceramidase results in ceramide species in the adipose and improved total body glucose homeostasis and insulin sensitivity under HFD feeding

A) Analysis of ceramide species of the indicated chain lengths from mesenteric (m), gonadal (g) and subcutaneous (s) fat pads from Art-AC mice and WT littermates. **B)** Analysis of total ceramide and sphingoid species from serum of Art-AC and WT littermates . **C)** Circulating glucose levels were measured during an oral glucose tolerance test (OGTT) (2.5 g/kg glucose per oral gavage). **D)** Serum insulin levels before and 15 minutes after oral glucose. **E)** Circulating glucose levels measured during an insulin tolerance test (ITT) (0.75 U/kg). **F)** Glucose infusion rates during hyperinsulinemic-euglycemic clamp experiments performed on conscious unrestrained 14-week-old WT and Alb-AC males (n = 6 mice). **G)** Hepatic glucose efflux during hyperinsulinemic-euglycemic clamp experiments performed on conscious unrestrained 14-week-old WT and Alb-AC males (n = 6 mice). **H)** Representative immunoblots of phosphorylated and total Akt of insulin-stimulated livers and gWAT of WT and Art-AC mice, shown in triplicate. **I)** 2-deoxyglucose uptake into fat pads of WT mice and Art-AC mice was assessed during the hyperinsulinemiceuglycemic state (n=6 per group). All samples are from Alb-AC mice and WT littermates after 8 weeks of HFD –dox challenge (n = 6-8 per group). *P<0.05, **P<0.01, ***P<0.001 by Student's t test.

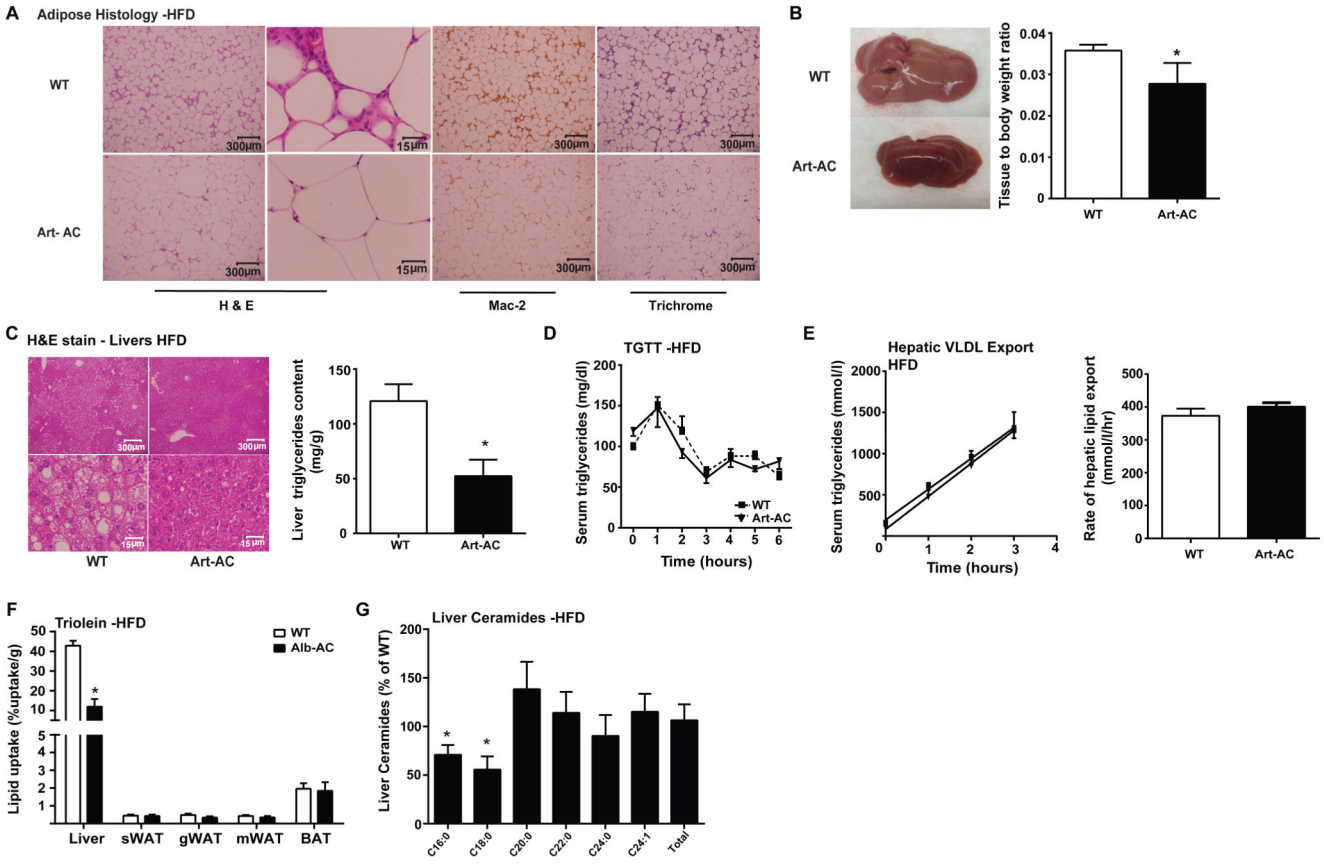

Fig. 4. Adipose-specific overexpression of acid ceramidase significantly reduces hepatic lipid accumulation and improves adipose tissue metabolic health when challenged with HFD

A) Representative images of H&E, Mac-2, and trichrome staining of WT and Art-AC gonadal fat pads. **B)** A representative gross image of WT and Art-AC livers. Bar graphs on the right represent the mass of the liver normalized to the total body weight of the mice. **C)** Representative H&E stained images of WT and Art-AC livers. Bar graphs on the right represent biochemical quantification of liver triglyceride levels. **D)** Circulating triglyceride (TG) levels were measured during an oral TG clearance test (20% intralipid, 15 uL/g body weight; single gavage) in Art-AC mice and WT littermate controls. **E)** Circulating triglyceride levels and the rate of hepatic VLDL export were measured following intravenous injection of tyloxapol (500 mg/kg) to inhibit plasma VLDL clearance in Alb-AC mice and WT littermate controls. **F)** Total ^{3}H-triolein lipid-uptake per tissue in WT and Alb-AC males 15-minutes after injection. **G)** Liver ceramide species and total ceramides were quantified and presented relative to wt levels of the same lipid species. All samples are from Art-AC mice and WT littermates after 8 weeks of HFD–dox challenge (n = 6-10 per group). **P*<0.05 by Student's *t* test.

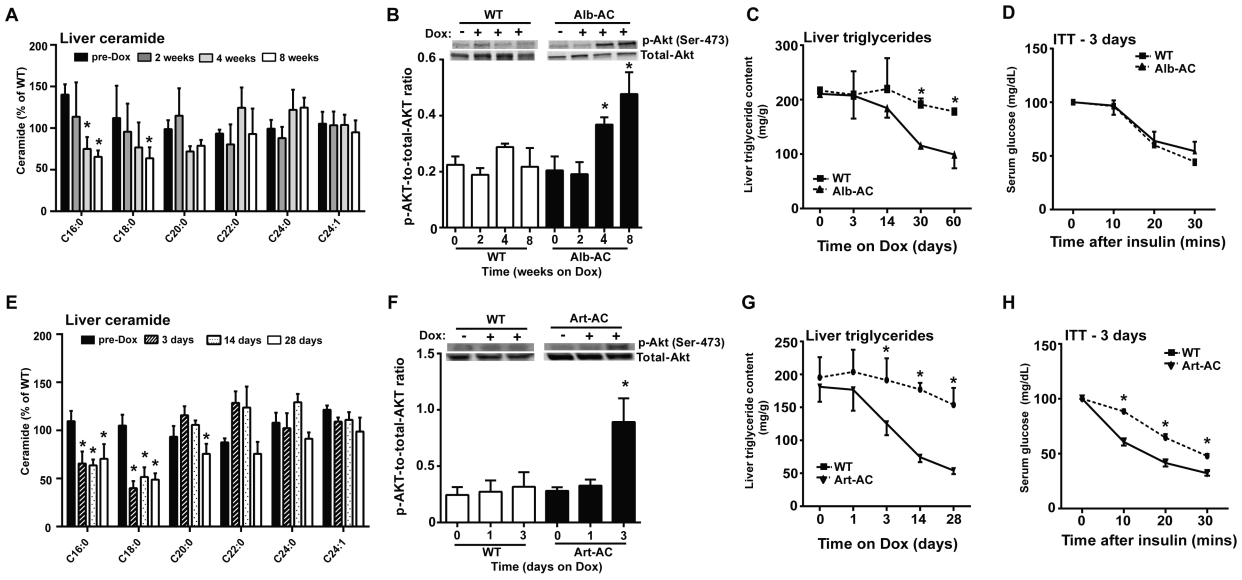

Fig. 5. Induction of acid ceramidase significantly improves insulin signaling and rescues hepatic steatosis in mice with diet induced obesity

All mice were maintained on high fat diets for 8 weeks prior to treatment with doxycycline. **A)** Liver ceramide species levels were quantified by tandem MS/MS for mice at pre-Dox treatment, 2 weeks, 4 weeks, and 8 weeks post-Dox treatment (n=4 at each time). **B)** Representative immunoblots of phosphorylated and total Akt from liver of insulin-stimulated WT and Alb-AC mice at pre-Dox treatment, at 2 weeks, 4 weeks, and 8 weeks post-Dox treatment (n=4 at each time). **C)** Liver triglycerides were quantified at different time points before or after Dox treatment (n=4 at each time). **D)** Circulating glucose levels measured during an insulin tolerance test (ITT) (0.75 U/kg) 3 days after HFD-dox treatment (n=4). **E)** Ceramides were quantified from liver of WT and Art-AC mice at pre-Dox treatment, 3 days, 14 days, and 28 days of doxycycline treatment (n=5 at each time). **F)** Representative immunoblots of phosphorylated and total Akt from liver of insulin-stimulated WT and Art-AC mice at pre-Dox treatment, at 24 hours, and 72 hours post-Dox treatment (n=4 at each time). **G)** Liver triglycerides were biochemically measured before and at the indicated time points after doxycycline addition to the diet in WT and Art-AC mice (n=6-10 at each time). **H**) Insulin tolerance tests were performed 3 days after doxycycline treatments in WT and AC-Art littermates (n=5). **P*<0.05 by Student's *t* test.

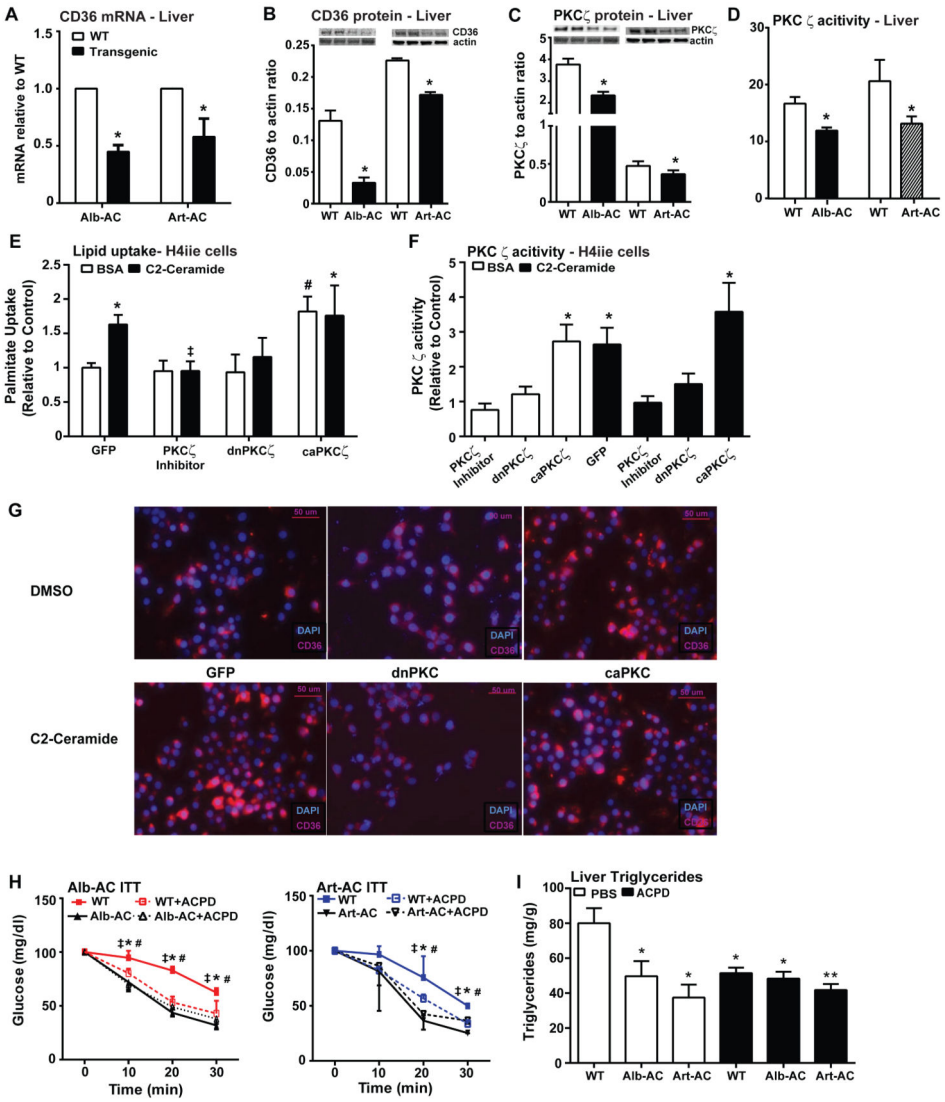

Fig. 6. Ceramides facilitate lipid uptake by mechanisms involving activation of PKCζ and CD36

A) Relative abundance of CD36 mRNA was assessed by qPCR from livers of WT, Alb-AC, and Art-AC mice following 8 weeks of HFD-dox. **B)** Hepatic expression of CD36 was assessed by Western blotting, and representative results are shown in duplicate. **C)** Hepatic expression of PKCζ were assessed by western blotting and representative results are shown in duplicate. **D)** PKCζ activity was assessed from livers of WT, Alb-AC, and Art-AC mice following 8 weeks of HFD-dox. **E-F)** Following transfection with GFP, dnPKCζ, or caPKCζ H4IIe hepatocytes were treated with C2-ceramide (100 M, in 0.2% BSA) or BSA for 1 hour prior to assessment of ^{3}H-palmitate uptake. Myristoylated PKCζ pseudosubstrate inhibitor was included for 90 minutes prior to ceramide treatments in non-transfected cells (n=4-8 from separate experiments). **F)** PKCζ activity was assessed from cell lysates harvested from cells represented in panel D. ‡ corresponds to comparison of C2-Ceramide treated cells with or without the PKCζ inhibitor. # corresponds to comparison of BSA treated cells that was transfected with either GFP or caPKCζ. **G)** Representative immunofluorescence of CD36 in

H4IIe cells transfected with GFP, dnPKCζ, or caPKCζ. Each group is treated with either DMSO or C2-Ceramide. **H)** Circulating glucose levels measured during an insulin tolerance test (ITT) (0.75 U/kg) of Alb-AC or Art-AC mice and littermate controls after daily injections of ACPD. * corresponds to comparison of WT to Alb or Art-AC. ‡ corresponds to comparison of WT and WT + ACPD. # corresponds to comparison of WT and Alb or Art-AC + ACPD. **I)** Biochemical quantification of hepatic lipid accumulation in Alb-AC or Art-AC mice and littermate controls after daily injections of ACPD. *,‡,#: $P<0.05$, **$P<0.01$ by Student's *t* test.

Table1

Metabolic parameters before and during hyperinsulinemic-euglycemic clamp study in WT and AC transgenics.

	Body weight (g)	Basal				Clamped			
		Plasma glucose (mg/dL)	Plasma insulin (ng/mL)	Plasma NEFA (mmol/L)	Plasma Glycerol (mg/mL)	Plasma glucose (mg/dL)	Plasma insulin (ng/mL)	Plasma NEFA (mmol/L)	Plasma Glycerol (mg/mL)
WT	49.4±1.8	208.2±7.8	0.87±0.13	0.47±0.06	0.41±0.04	177.4±5.1	3.58±0.47	0.33±0.06	0.47±0.11
Alb-AC	48.8±2.0	191±3.9	0.83±0.13	0.42±0.03	0.32±0.02	168±6.5	4.2±0.72	0.27±0.07	0.38±0.13
WT	30.8±1.6	207±2.4	0.98±0.1	0.51±0.08	0.59±0.15	153.9±4.6	3.4±0.61	0.51±0.06	0.41±0.1
Art-AC	30.9±1.06	174.2±23.3	0.66±0.16	0.42±0.04	0.38±0.09	142.7±3.5	3.4±0.5	0.34±0.08	0.36±0.09